Impact of calcium binding and thionylation of S100A1 protein on its NMR derived structure and backbone dynamics

Journal:	*Biochemistry*
Manuscript ID:	bi-2012-015407.R2
Manuscript Type:	Article
Date Submitted by the Author:	n/a
Complete List of Authors:	Nowakowski, Michał; University of Warsaw, Faculty of Chemistry Ruszczynska-Bartnik, Katarzyna; Institute of Biochemistry and Biophysics, Polish Academy of Sciences, Laboratory of Biological NMR Budzinska, Monika; Institute of Biochemistry and Biophysics, Polish Academy of Sciences, Laboratory of Biological NMR Jaremko, Lukasz; University of Warsaw, Faculty of Chemistry; Institute of Biochemistry and Biophysics, Polish Academy of Sciences, Laboratory of Biological NMR Jaremko, Mariusz; Institute of Biochemistry and Biophysics, Polish Academy of Sciences, Laboratory of Biological NMR Zdanowski, Konrad; Institute of Biochemistry and Biophysics, Polish Academy of Sciences, Laboratory of Biological NMR Bierzynski, Andrzej; Institute of Biochemistry and Biophysics, Polish Academy of Sciences, Biophysics Ejchart, Andrzej; Institute of Biochemistry and Biophysics, Polish Academy of Sciences, Laboratory of Biological NMR

Impact of calcium binding and thionylation of S100A1 protein on its NMR derived structure and backbone dynamics †,‡

Michał Nowakowski,[§,^,#,] Katarzyna Ruszczyńska-Bartnik,[§,#] Monika Budzińska,[§,#] Łukasz Jaremko,[§,||] Mariusz Jaremko,[§] Konrad Zdanowski,[§,⊥] Andrzej Bierzyński,[§] and Andrzej Ejchart[§]*

[§]Institute of Biochemistry and Biophysics, Polish Academy of Sciences, Pawińskiego 5A, 02-106 Warsaw, Poland, [||]Faculty of Chemistry, Warsaw University, Pasteura 1, 02-093, Warsaw, Poland, [⊥]Institute of Chemistry, University of Natural Sciences and Humanities, 3 Maja 54, 08-110 Siedlce, Poland, ^present address Faculty of Chemistry, Warsaw University, Pasteura 1, 02-093, Warsaw, Poland, [#] these authors contributed equally to this work, * Corresponding author. Phone: +48 22 8220211 421. Email: lyam@chem.uw.edu.pl.

† This work was supported by grants from the Ministry of Science and Higher Education (N301/031234 and N301/122438) and the Iuventus Plus program (project nr IP2010014570, to Ł. J.).

‡ The coordinates for the human *holo*-S100A1 and *holo*-S100A1-Hcy structures have been deposited in the Protein Data Bank (accession numbers 2LP3 and 2LP2, respectively). The ^{1}H, ^{13}C and ^{15}N resonance assignments and ^{15}N magnetic relaxation data have been deposited in the BioMagResBank (accession numbers 18231 and 18230, respectively).

[1] Abbreviations: CPMG, Carr – Purcell – Meiboom – Gill pulse train; CSI – chemical shift index; CSP – chemical shift perturbation; DSS-d_4, 3-trimethylsilyl-2,2,3,3-tetradeuteropropionic acid sodium salt; EDTA, ethylenediaminetetraacetic acid; HSQC, heteronuclear single quantum coherence; HPLC, high performance liquid chromatography; TRIS-d_{11}, perdeuterated 2-amino-2-(hydroxymethyl)1,3-propanediol.

Abstract

S100 proteins play a crucial role in multiple important biological processes in vertebrate organisms acting predominantly as calcium signal transmitters. S100A1 is a typical representative of this family of proteins. Upon binding of four Ca^{2+} ions it undergoes a dramatic conformational change, resulting in exposure, in each of its two identical subunits, a large hydrophobic cleft that binds to target proteins. It has been shown that abnormal expression of S100A1 is strongly correlated with a number of severe human diseases: cardiomyopathy and neurodegenerative disorders.

A few years ago we have found that thionylation of Cys 85 - the unique cysteine in two identical S100A1 subunits – leads to a drastic increase of the protein affinity for calcium. We postulated that the protein activated by thionylation becomes a more efficient calcium signal transmitter. Therefore, we decided to undertake, using NMR methods, a comparative study of structure and dynamics of native and thionylated human S100A1 in its *apo* and *holo* states. In this paper we present the results obtained for the both forms of this protein in its *holo* state and compare them with the previously published structure of native *apo* S100.

The main conclusion that we draw from these results is that the increased calcium binding affinity of S100A1 upon thionylation arises, most probably, from rearrangement of the hydrophobic core in its *apo* form.

Introduction

A large number of papers on structure and biological function of S100 proteins can be found in the literature and every year this number increases dramatically. There is a good reason for that: these proteins, acting predominantly as calcium signal transmitters, have been shown to play a crucial role in multiple important biological processes in vertebrate organisms [1].

S100A1 is a typical S100 protein. It is a homodimer composed of noncovalently bound, antiparallely oriented, subunits. Each of them is build of two so called "EF hand" motives bound together by a short linker. The N-terminal motives contain a 14 residue long calcium binding loop, specific for S100 proteins, flanked by two α-helices (helix I and helix II). The C-terminal ones coordinate Ca^{+2} ions by a "canonical" loop, ubiquitous in calcium binding proteins, formed by 12 amino acid residues situated in between helix III and helix IV.

Upon Ca^{2+} binding the protein undergoes a dramatic conformational change, resulting in exposure, in each of its subunits, a large hydrophobic cleft formed by residues situated in the linker, the C terminus, and helix III [2]. Numerous structural studies indicate that this region is responsible for recognition of S100 target proteins [3].

S100A1 is highly expressed in human heart muscle and brain. It is also found in skeletal muscles and kidney. It has been shown that abnormal expression of this protein is strongly correlated with a number of severe human diseases: cardiomyopathy, and neurodegenerative disorders such as Alzheimer disease [4-7].

A few years ago we have found that thionylation of Cys 85 - the strictly conserved, unique cysteine residue of S100A1 subunits by small thiol molecules such as β-mercaptoethanol, glutathione or cysteine leads to a dramatic increase of the protein affinity

for calcium [8]. It prompted us to formulate the hypothesis that S100A1 can play the role of a linker between calcium- and redox-signal pathways.

Protein S-thionylation is the posttranslational modification of cysteine residues by forming a mixed disulphide between cysteine thiol group and low molecular mass endogenous thiols. At present, a large number of proteins undergoing thionylation has been described [9]. Thionylation of proteins has been shown to regulate activities of enzymes, transcriptional factors, cell surface receptors, and cytoskeletal proteins. It plays an essential part in the control of cell-signalling pathways associated with viral infections and with tumour necrosis factor [10]. The thionylation has been also suggested as a mechanism through which protein functions can be regulated by the redox status [11].

To elucidate the molecular mechanism of S100A1 activation due to thionylation we decided to undertake, using NMR methods, a precise comparative study of structure and dynamics of human S100A1 protein, native and with thionylated Cys 85 residue, in its *apo* and *holo* states.

Knowledge of static 3D structures of proteins, while extremely important, is not sufficient to fully understand the function of proteins and their interactions in complexes. It is believed that intramolecular motions in proteins are one of the most important factors which determine their basic physico-chemical properties, biological activity, and also interactions with ligands, receptors or nucleic acids. Magnetic relaxation of ^{15}N amide nuclei allows to monitor motions of protein backbone within the wide range of time scales. This approach of probing dynamics of N–H groups allows characterization of motions over most of protein backbone [12-13].

The results obtained by us for human *apo* S100A1 have already been published [14]. In the current paper we discuss the structure and dynamics of the *holo* form of this protein and its mixed disulfide with homocysteine.

The choice of homocysteine can seem rather puzzling: glutathione is by far the most abundant thiol molecule in vertebrate organisms and, therefore, the most likely to form mixed disulfides with proteins. On the other hand, homocysteine is situated at a critical regulatory branch point in sulfur metabolism. It can be remethylated to methionine, an important amino acid in protein synthesis, or converted to cysteine in the transsulfuration pathway [15]. It has been shown that homocysteine has the highest tendency to create disulfide bonds with proteins among such thiols as homocysteine, cysteine and glutathione in HeLa cell cultures. Such S-homocysteinylation impairs the function of many enzymes, structural proteins and receptors disturbing many metabolic functions in the cell [16]. It has been also shown that homocysteine administered orally resulted in the increase of protein-bound homocysteine in plasma with a concurred decrease in protein-bound cysteine, suggesting displacement of bound cysteine [17]. Elevated level of homocysteine is associated with the increased risk of cardiovascular disease [18], cerebrovascular disease, Alzheimer disease, neural tube defects, osteoporosis, renal failure, and diabetes. Homocysteine can form mixed disulfides with plasma proteins, such as albumin, transthyretin, fibronectin or lipoprotein(a) as well as with intracellular proteins like metallothionein or glutathione peroxidase [19]. Therefore, homocysteinylation of S100A1, while not reported yet, might be a biologically important phenomenon: high levels of homocysteine are considered to be risk factors in the same disorders which are linked with abnormal S100A1 expression [20-21].

Materials and Methods

Sample preparation

^{15}N-labeled and ^{13}C,^{15}N-double labeled S100A1 protein was obtained as previously described [14, 22]. Expression products were isolated using the classical method of ammonium sulfate precipitation [23-24], purified by reversed-phase HPLC on a semipreparative Vydac C18 column, and identified by electrospray ionization mass

spectrometry using a Macromass Q-Tof spectrometer. Two forms of the protein, one with the sequence strictly corresponding to its gene sequence and another one, with the additional initiator methionine at the N-terminus, were obtained from HPLC as partly overlapping peaks. NMR measurements indicated that structural differences between both forms are small and restricted to the close proximity of the N-terminal Met residue [14, 25]. Therefore, a mixture of both forms of proteins was used in all experiments. Thionylation of S100A1 protein with homocysteine (disulfide bond formation between cysteine 85 and homocysteine, S100A1-Hcy) was performed in 0.2 M TRIS buffer containing 5 M GuHCl, 5 mM EDTA and 5 mM homocystine disulfide at pH 8.5. The reaction was carried out at room temperature for 50 min. The modified protein was purified by HPLC and identified by electrospray ionization mass spectrometry. NMR samples of 650 μL volume contained 0.8 - 1.0 mM protein solution (monomer concentration) in 90%/10% H_2O/D_2O, 50 mM TRIS-d_{11}, 10 mM $CaCl_2$, 0.1mM NaN_3 and 50 mM NaCl with pH adjusted to 7.2 (uncorrected value). In case of H_C detected experiments 100% deuterated buffer was used.

NMR spectroscopy

All NMR measurements were performed at the temperature carefully adjusted to 37°C checked by an ethylene glycol reference sample. Time domain data were acquired using the States-TPPI quadrature detection [26] followed by the sensitivity enhanced detection introduced by L. E. Kay [27]. 1.6 s recycling delay was used, if not stated otherwise. All chemical shifts in ^1H NMR spectra were reported with respect to external DSS-d_4. Chemical shifts of ^{13}C and ^{15}N signals were referenced indirectly using the 0.251449530 and 0.101329118 frequency ratios for $^{13}C/^1H$ and $^{15}N/^1H$, respectively [28]. Experimental data were processed using the NMRPipe software package [29]. Zero filling and 90° shifted squared sine-bell filter were applied prior to the Fourier transformation. Processed spectra were analyzed with both the CARA [30] and the SPARKY [31] software.

The sequence-specific assignments were performed using uniformly ^{13}C,^{15}N-double labeled samples of *holo*-S100A1 and *holo*-S100A1-Hcy. 3D heteronuclear HNCO [32], HNCA [33], HN(CO)CA [34], HNCACB [35], CBCA(CO)NH [36], and (HCA)CO(CA)NH [37] spectra were used to obtain assignments of the backbone ^{1}H, ^{13}C and ^{15}N resonances. The assignments were additionally confirmed by analysis of sequential and medium-range NOE signals in the respective 3D ^{15}N-edited NOESY-HSQC spectra [38]. The aliphatic side chain ^{1}H and ^{13}C resonances were assigned from the analysis of the ^{1}H–^{13}C HSQC, C(CO)NH [39], HBHA(CBCACO)NH [40], HCCH-TOCSY [41], (H)CCH-TOCSY [41], and ^{13}C-edited NOESY-HSQC spectra [42]. The aromatic side chain resonances were assigned from the (HB)CBHD, (HB)CBHE [43], ^{1}H–^{13}C HSQC, and ^{13}C-edited NOESY-HSQC spectra recorded with the offset, spectral widths and ^{13}C–^{1}H coupling constants tuned to aromatic carbons. Distance constraints were obtained from the ^{15}N-edited NOESY-HSQC spectra and the ^{13}C-edited NOESY-HSQC spectra separately tuned to aliphatic and aromatic carbons.

Longitudinal (R_1) and transverse (R_2) relaxation rates were measured at three magnetic fields: 9.4, 11.7 and 16.4 T, with ^{15}N-labeled sample using the sensitivity enhanced ^{1}H–^{15}N HSQC pulse sequence [27] with the option of either R_1 or R_2 measurements of ^{15}N nuclei [44]. The R_2 relaxation rate measurements were performed with the CPMG pulse train. A refocusing time of 650 μs was used during the evolution delays. The acquisition parameters for R_1 and R_2 measurements on each spectrometer were identical with the exception of the delay between π (^{1}H) pulses used for the cross-correlation effect suppression [45]. 5 and 10 ms delays were used in the R_1 and R_2 measurements, respectively. Delays between the scans of 1.8 s were employed in both types of experiments. {^{1}H}–^{15}N NOEs were measured with the pulse sequence included in the ProteinPACK Varian Inc. (Palo Alto, CA) software at 16.4 T for *holo*-S100A1 and at 9.4 and 16.4 T for *holo*-S100A1-Hcy.

Resonance intensities were used in calculating relaxation rates and NOE values. Experimental errors of relaxation rates were obtained from appropriate elements of the variance-covariance matrix. Experimental errors in NOE values were evaluated from signal-to-noise ratios obtained for corresponding signals in spectra with and without NOE [46].

The ^{1}H, ^{13}C and ^{15}N resonance assignments and ^{15}N magnetic relaxation data have been deposited in the BioMagResBank with the accession codes 18231 (*holo*-S100A1) and 18230 (*holo*-S100A1-Hcy).

Structure calculations

The NOESY interproton distance constraints were derived from the 3D heteronuclear ^{15}N- and ^{13}C-edited NOESY-HSQC experiments. The initial structure calculations were performed with the CYANA 3.0 software [47]. The dimeric interface between the protein subunits was defined basing on structural similarity to the known structure of rat S100A1 protein [2] (PDB entry 1ZFS). The automatic NOESY assignment procedure [48] provided 1193 intrasubunit distance constraints and 121 intersubunit distance constrains for *holo*-S100A1 protein. Appropriate numbers for *holo*-S100A1-Hcy were 1240 and 156, respectively. Stereospecific assignments for 74 (*holo*-S100A1) or 100 (*holo*-S100A1-Hcy) side chain chiral groups in each subunit were generated by the program GLOMSA [49] that is included in the CYANA software. Additional restraints for backbone φ and ψ torsion angles for Ser 2–His 18, Leu 28–Glu 63, and Val 69–Thr 82 segments were predicted from the chemical shifts using the PREDITOR server [50]. For the less defined protein regions (like Ser 19–Lys 27 and Asn 64–Glu 68 calcium binding loop segments or the C-terminus of helix IV starting from Val 83) the dihedral angle constraints were not applied. At first, the structure calculations were carried out using the XPLOR-NIH 2.26 program [51] with NOEs and dihedral angles as input constraints assuming the symmetry equivalence between two subunits. Before the final structure calculations, constraints defined as $r_{HN\text{-}O}$ = 1.5–2.5 Å and

r_{N-O} = 2.5–3.5 Å for hydrogen bonds were added based on geometric criteria. If a given hydrogen bond existed in more than 75% of structures in the ensemble, then it was selected for the final refinement. Additional 20 constrains, defined as r_{Ca2+-O} = 2.33–2.47 Å for calcium ions coordination, were also included in final refinement. Only oxygen atoms taking part directly in calcium coordination were selected (O of Ser 19, Glu 22, Asp 24, Lys 27 and OE1, OE2 of Glu 32 for the first binding site, and OD1 of Asp 62, Asn 64, OD1, OD2 of Asp 66, O of Glu-68, and OE1, OE2 of Glu 73 for the second binding site), on the basis of the representative crystallographic structures of human S100A13 (PDB entry 2EGD) and bovine S100B (PDB entry 1MHO). For the purpose of final refinement of *holo*-S100A1-Hcy structure, the topology of an additional amino acid, homocysteine connected to cysteine by the disulfide bond, was manually added and included in XPLOR-NIH 2.26 topology file. Evaluation of the obtained S100A1 structures quality was done with the PROCHECK-NMR [52] and the What-If [53] programs.

Analysis of ^{15}N relaxation data

Methodology of analyzing ^{15}N relaxation data measured at multiple magnetic fields has been described in our previous paper [14]. It is based on the extended model-free approach [54] with spectral density functions combined [55-56] with anisotropic overall tumbling [57].

Three Euler angles relate the directions of the principal axes of the asymmetric diffusion tensor to the molecule-fixed coordinate system. Because of the symmetry requirement one of the principal axes of the diffusion tensor of homodimeric S100A1 protein (in our case *z* axis) is collinear with the protein symmetry axis. This condition reduces the number of the Euler angles from three to one. The coefficients describing orientation of H–N vectors in the molecule-fixed coordinate system were calculated using the atomic coordinates of the lowest energy NMR-derived structures. The vibrationally averaged N–H distance was

assumed to be 0.104 nm [58] and chemical shift anisotropy of ^{15}N chemical shift tensor equal to –170 ppm [59]. The values and ratios of the principal values of inertia tensors are given in Supporting Information, Table S1 and compared with the *apo* form of S100A1 protein. Anisotropies of the inertia moment tensors are noticeable and, therefore, anisotropic overall tumbling may be expected.

The least-squares procedure used a written in-house Fortran routine optimizing the model parameters consisted of minimization through a grid-search of the target function χ given by:

$$\chi = \sum_{i=1}^{N} \sum_{j=1}^{M} [(P_{ij,exp} - P_{ij,calc})^2 / \sigma_{ij}^2]$$

The sum was over M relaxation parameters for each of N residues, and $P_{ij,calc}$ were the appropriate relaxation parameters calculated from the assumed model. The σ_{ij} values were the corresponding standard deviations of experimentally derived $P_{ij,exp}$. The minimization procedure delivered four global parameters (three diffusion coefficients and one Euler angle) and N sets of local, residue specific, parameters comprising S_f, S_s, τ_f, τ_s, and R_{ex}. The residues of both flexible termini were also excluded from the calculation delivering the overall diffusion parameters. Those unstructured, flexible terminal segments cannot be regarded as a part of the rigid rotor and description of their motions in terms of a single overall correlation time does not seem to be appropriate [60-61]. Model parameter uncertainties derived in the minimization of target function χ were obtained as standard deviations from 200 Monte Carlo simulations [62].

Results

Sequence-specific resonance assignment

The 2D ^{1}H-^{15}N HSQC spectra of both homodimeric S100A1 proteins displayed relatively good dispersion of amide correlation signals (cf. Fig. 1). In *holo*-S100A1-Hcy cross peaks for all residues could be assigned, except 5 residues placed, respectively, in the N-terminus (Ser 2), the N-binding loop (Gly 23, Asp 24, and Lys 25) and the linker (Lys 49). In *holo*-S100A1 the cross peaks of the same residues and additionally of three other ones (Leu 41, Asn 86 and Asn 92) could not be identified because of line broadening caused, most probably, by exchange processes. The sequence-specific backbone and side-chain assignments were done using 2D and 3D NMR experiments. 91.4% of all resonances in *holo*-S100A1 and 89.8% in *holo*-S100A1-Hcy were assigned. All resonances, except those of histidine rings and NH_2 side chain groups of asparagines and glutamines, have been assigned unequivocally. The $^{13}C_\beta$ chemical shift of Cys 85 in *holo*-S100A1-Hcy (δC_β=40.6), as compared with that in *holo*-S100A1 (δC_β=26.5), clearly shows that the protein was thionylated [63-64] but the resonance assignment for the unlabeled homocysteine was not possible.

Effect of calcium binding on the ^{1}H-^{15}N HSQC spectrum of S100A1

It is well known that saturation with calcium changes significantly many of the chemical shifts in S100 proteins [2]. In human S100A1 prominent examples are those of Glu 63 and Gly 67 occupying the second and sixth position of "canonical" calcium-binding loop. Their cross peaks in the ^{1}H-^{15}N HSQC spectrum move, respectively, from 118.86 ppm/8.09 ppm and 109.02 ppm/8.22 ppm [14] to 129.19 ppm/8.35 ppm and 113.25 ppm/10.27 ppm (this paper) upon calcium binding. Coordination of Ca^{2+} ions by S100A1 is also manifested by more general changes in the chemical shifts of the protein backbone amide nuclei in the ^{1}H-^{15}N HSQC spectra upon saturation of the *apo*-protein with calcium ions. The chemical shift perturbation (CSP) upon binding of Ca^{2+} ions was calculated for each residue using the equation: $CSP = [(\Delta\delta_{HN})^2 + (0.2\ \Delta\delta_N)^2]^{1/2}$ where $\Delta\delta_{HN}$ and $\Delta\delta_N$ are

chemical shift changes in proton and nitrogen dimensions, respectively. CSP values are shown in Supporting Information, Fig. S1. The largest changes are observed for both binding loops. Pronounced changes are also visible for the linker - particularly for its first residue, Ser 42 - and the C-terminal part of helix IV. On average, CSPs equal to 0.69 ppm for both pairs: *apo*-S100A1/*holo*-S100A1 and *apo*-S100A1/*holo*-S100A1-Hcy. Both CSP profiles mapped onto appropriate protein structures are given in Supporting Information, Fig. S2. A similar calcium-induced chemical shift perturbation profile was observed in the case of human S100A5 protein [65].

Structures of *holo*-S100A1 and *holo*-S100A1-Hcy

The three-dimensional solution structures of the human *holo*-S100A1 protein and its derivative modified by disulfide formation with homocysteine at Cys 85 (*holo*-S100A1-Hcy) were calculated from NMR-derived constraints (cf. Table 1). 99.2 % (99.6 %) of all residues are located in the most favored 95.1% (95.9%) or additionally allowed regions 4.1% (3.7%) of the Ramachandran plot. The statistics for the ensembles of 20 most favorable structures for both proteins are given in Table 1. In Fig. 2 the ribbon diagrams for the lowest energy structures of *holo*-S100A1 (Fig. 2A) and *holo*-S100A1-Hcy (Fig.2B) are shown with color-encoded EF-hand helices. The atomic coordinates for all 20 structures of each protein have been deposited in the Protein Data Bank with the accession codes 2LP3 for human *holo*-S100A1 and 2LP2 for *holo*-S100A-Hcy, respectively.

The structures of both proteins are almost identical, as could be expected from comparison of their ^{1}H-^{15}N HSQC spectra: the average chemical shift perturbation CSP for the *holo*-S100A1/*holo*-S100A-Hcy pair equals merely 0.04 ppm (cf. Fig. S1C) and it arises predominantly from local effects of the protein thionylation. Each subunit of *holo*-S100A1 (*holo*-S100A1-Hcy) contains four α-helices formed by residues Glu 3–Gly 20 (Lys 21), Lys 30–Glu 40, Ala 53–Leu 61 and Phe 71–Glu 91 (Trp 90) and one short antiparallel β-sheet

formed by Lys 27, Leu 28, Val 69, and Asp 70. In the linker region joining two EF-hand domains (residues 41 - 50) of *holo*-S100A1-Hcy the α-helix is formed consisting of Gly 43–Asp 46. Such short helical motif does not appear in *holo*-S100A1 proteins of both, human (this work) and rat [2] species.

For residues Glu 5–Cys 85 within one subunit of *holo*-S100A1 (*holo*-S100A1-Hcy), the r.m.s.d. for the backbone atoms (N, C_α, C') equals 0.86 ± 0.22 Å (0.44 ± 0.10 Å) and for all heavy atoms 1.49 ± 0.26 Å (0.85 ± 0.12 Å), while for both subunits in the dimer the corresponding values are 0.94 ± 0.22 Å (0.54 ± 0.14 Å) and 1.54 ± 0.27 Å (1.04 ± 0.15 Å), respectively. Almost identical r.m.s.d. values obtained for the single subunit and the homodimer in both proteins prove that the interface between subunits is correctly determined and the resulting ensembles of structures represent well defined homodimeric proteins. In both proteins the dimer interface is located mainly between helices I and I', I and IV' and helices IV and IV'. On average 4 – 5 long-range distance restraints have been established from the NOE data for residues involved in the dimer formation.

Dynamics of *holo*-S100A1 and *holo*-S100A1-Hcy

For *holo*-S100A1 and *holo*-S100A1-Hcy proteins the analysis of relaxation data was performed for 73 and 66 residues, respectively, allowing for the simultaneous determination of four global parameters and corresponding sets of local parameters. The principal values of the overall diffusion tensors are collected in Supporting Information, Table S2. As supposed the overall tumbling is anisotropic with anisotropy $D_A = 2D_z/(D_x+D_y)$ equal to 0.78±0.01 and 0.88±0.04 for *holo*-S100A1 and *holo*-S100A1-Hcy, respectively. Anisotropy of the overall tumbling in *apo*-S100A1 is less pronounced and equal to 0.92±0.02. The averaged isotropic rotational correlation time, $\tau_R = (2D_x+2D_y+2D_z)^{-1}$, equal to 9.50±0.08 ns and 9.27±0.20 ns for *holo*-S100A1 and *holo*-S100A1-Hcy, respectively, is typical for globular proteins of about 20 kDa size and corresponds well to the results obtained for other proteins from the S100 family

[14, 65-68]. Comparison of the *apo* and *holo* forms reveals that overall tumbling of *holo* forms is ca. 10% slower. It should not be surprising in the light of larger molecular inertia moments of *holo* forms (cf. Supporting Information, Table S1).

Out of five residue-specific parameters describing the local mobility of the backbone amide N–H vectors within the frame of the extended model-free approach, $S^2 = S_f^2 S_s^2$ and R_{ex} are of special importance. The former describes restrictions imposed on motions much faster than the overall protein diffusion (the ps time scale) and the latter allows detection of much slower motions, but fast enough to average chemical shifts of the exchanging sites (usually on the μs–ms time scale). Site specific values of those parameters can reveal local dynamics changes due to the thionylation and calcium loading for both studied proteins when compared with corresponding values in *apo*-S100A1 [14]. However, differences in mobility of the protein structural elements (helices, loops) on the ps time scale become much more evident when the weighted means of S^2 values determined for the residues building them are compared.

The S^2 values averaged over structural elements presented in Fig. 3 indicate that the helices are always the most rigid segments of the studied proteins (full profiles of site specific S^2 values are given in Supporting Information, Fig. S3). Rigidity of both binding loops in the *holo* forms is comparable to that of helices. On the other hand, the linker is the most flexible part of the molecule, much more flexible than in the *apo* form. In the *holo* forms residues involved in chemical exchange processes monitored by the R_{ex} parameter (Fig. 4) are predominantly located in the helices I and II and the linker in contrary to the most affected by exchange processes N-terminal binding loop in *apo* form.

Residues of binding loops differ in their dynamic behavior between the *holo* and *apo* forms. In the latter structure, the residues located in the binding loops display intense mobility on the ps time scale comparable to that of the linker. Moreover, they show the exchange terms

being the largest in the N-terminal loop. Therefore, calcium binding imposes restriction on the mobility of residues comprising binding loops on fast and slow time scales. On the contrary, the mobility of the linker, on both time scales, and of large parts of helices I and II on slow time scale becomes more pronounced in the *holo* forms.

The obtained model parameters reproduce well input experimental data. The plot of calculated vs. experimental R_2/R_1 ratios is given in Supporting Information, Fig. S4.

Discussion

Impact of calcium binding on human S100A1 structure and its backbone dynamics

The structural transition in human S100A1 protein induced by calcium binding is strictly similar to that observed in rat S100A1 [2, 69] and characteristic for the majority of S100 proteins [65, 70]: helix III changes its orientation by ca. 100° (cf. Table 2 and Fig. 5) that leads to the creation of a large hydrophobic cleft on the surface of the protein comprising the residues situated in the linker, helix III, and helix IV. To this region of *holo*-S100A1 the target proteins bind [71-72].

From studies on rat S100A1 [2, 69] the authors have concluded that elongation of helix IV at its C-terminus is an additional structural change induced by calcium binding in the protein. A similar conclusion has been drawn from studies on human S100A5 [65]. In human *apo*-S100A1 [14] we have found one turn more in helix IV than reported for the rat *apo* protein [69] but the residues participating in its formation (Asn 87 - Trp 90) are in equilibrium between helical (3_{10}-helix) and non-helical conformation. In the *holo* forms of S100A1 presented in this paper the equilibrium is shifted toward the α-helical conformation.

As could be expected the striking difference in dynamics of *apo*-S100A1 and *holo*-S100A1 proteins is the significant restriction of motion of both calcium binding loops. S^2 values averaged over structural motifs are larger for calcium binding loops in *holo*-S100A1 (cf. Fig. 3). In calcium bound form those previously mobile on subnanosecond time scale

structural elements become as rigid as helices. In other words, quite expectedly calcium binding imposes restriction on fast motions of the loops. Additionally, the linker region in *holo*-S100A1 becomes more mobile and thionylation of Cys 85 enhances this effect. The latter phenomenon can be explained by possible interactions between attached homocysteine and residues within the linker (cf. Fig. 2B). Moreover, the analysis of differences in R_{ex} terms for those two proteins reveals that calcium binding restricts the mobility of S100 specific calcium binding loop. There is another feature that characterizes studied *holo* protein forms, namely the significant increase of exchange terms in helices I and II in comparison with *apo* form. This effect has not been reported for any of S100 proteins up to now. It points out to the increased mobility on the μs–ms time scale of secondary structure elements which usually remain rigid. This behavior can be a hallmark of the target binding site as recently reported for the S100A6 complex with a fragment of C-terminal domain of Siah-1 protein [3]. It was observed that complex formation resulted in both, chemical shift perturbation in H/N correlation spectrum and broadening or disappearing of numerous cross peaks corresponding to several regions of S100A6 including most of the residues within helix I. It can also correlate with the increased exchange rates of several amide protons with solvent within helices I and II of human [73] and rat [74] S100B proteins.

Comparison of *holo*-S100A1 structures

Until now there are three available structures of *holo*-S100A1 proteins: rat (1ZFS) [2] and presented in this paper human (2LP3) and human thionylated with homocysteine (2LP2). All these structures, determined by NMR methods, are very similar. The r.m.s.d. values calculated for backbone atoms of residues Glu 5 - Cys 85 in structure pairs 1ZFS/2LP3, 1ZFS/2LP2, and 2LP2/2LP3 equal to 1.92±0.20 Å, 2.24±0.11 Å and 1.63±0.09 Å, respectively. The positions of secondary structure elements as well as mutual orientations of helices (see Table 2) are also very similar in those three structures. The only structural

difference is visible in the linker region (residues Leu 41 - Asp 50). It does not contain any elements of secondary structure in rat and human *holo*-S100A1 proteins, while in *holo*-S100A1-Hcy an α-helix segment consisting of Gly 43–Gln 46 has been found. Nevertheless, we believe that it is simply more populated because in all these proteins the linker region is very flexible (see Fig. 3). Existence of a short α-helix in the linker region has been found in all crystallographic structures of calcium loaded S100 proteins [75-77]. Moreover, the chemical shift index (CSI) values of Cα nuclei obtained for all discussed here S100A1 proteins indicate that residues 42-46 (42-45 in rat S100A1) are likely to adopt the α-helical conformation (cf. Supporting Information, Fig. S5).

The results presented in this paper show that the protein thionylation is not reflected in any significant changes in the structure or dynamics of its *holo* form. Therefore, the rationale of increase of the protein affinity for calcium due to the thionylation of Cys 85 should be searched in conformational changes in its *apo* form.

Therefore, it seems obvious that we should to investigate this problem by thoroughly analyzing the structure of *apo*-S100A1-Hcy. Unfortunately, the signal dispersion in NMR spectra of this protein is very poor precluding spectral assignments at the level allowing for the precise structure determination. Nevertheless, at least partial assignment of a number of resonances was possible. It allowed us to identify C/H correlations for several aromatic moieties and calculate CSP values caused either by calcium binding or thionylation of the protein. The aromatic $^{1}H–^{13}C$ HSQC spectra, which can be regarded as fingerprints of the hydrophobic core arrangement, are virtually identical for both studied *holo* proteins (S100A1 and S100A1-Hcy) and the *apo* form of S100A1-Hcy, while the corresponding spectrum of native *apo* S100A1 markedly differs from them. Visual inspection of superpositions of selected pairs of 2D aromatic $^{1}H–^{13}C$ HSQC spectra (Supporting Information, Fig. S6) confirms this statement. Selected CSP values of aromatic C/H cross peaks and Nε1/Hε1 side

chain Trp residue are large and similar for *apo*-S100A1/*holo*-S100A1 and *apo*-S100A1/*apo*-S100A1-Hcy pairs. On the other hand, they are much smaller for the *apo*-S100A1-Hcy/*holo*-S100A1-Hcy pair (cf. Supporting Information, Table S3). One can conclude that the rearrangement of hydrophobic side chains of aromatic residues due to the protein thionylation reflected by aromatic C/H correlation spectrum of *apo*-S100A1-Hcy is similar to that resulting from calcium binding to S100A1. This conclusion is in line with our previous finding that Cys 85 thionylation stabilizes C-terminal part of helix IV in S100A1 protein [68] as does the calcium binding.

Conclusions

Loading of S100A1 protein with calcium results in stabilization of the C-terminal part of α-helix IV in addition to drastic reorientation of helix III. As could be expected, the calcium binding loops are much more rigid in the *holo* form of the protein.

Quite surprisingly, helices I and II and, in particular, the linker region in the *holo* form, are more flexible than in the *apo* form. It can be of functional importance facilitating molecular recognition of the protein target molecules.

Neither the structure nor the dynamics of *holo*-S100A1 are perceptibly affected by the protein thionylation. That leads to the following important conclusion: the observed increase of S100A1 affinity for calcium upon its Cys 85 thionylation results generally from conformational changes in the *apo* form of the protein which seem to arise from rearrangement of aromatic residues constituting its hydrophobic core.

Acknowledgements

We are grateful to Prof. Wiktor Koźmiński from Warsaw University, Poland, and Dr. Igor Zhukov from National Institute of Chemistry, Ljubljana, Slovenia for making high field NMR spectrometers available to us.

Supporting Information

Detailed information on structure and dynamics of studied proteins contains three tables and six figures. This material is available free of charge via the Internet at http://pubs.acs.org

References

1. Santamaria-Kisiel, L., Rintala-Dempsey, A.C., and Shaw, G.S. (2006) Calcium-dependent and -independent interactions of the S100 protein family, *Biochemical Journal* 396, 201-214.

2. Wright, N.T., Varney, K.M., Ellis, K.C., Markowitz, J., Gitti, R.K., Zimmer, D.B., and Weber, D.J. (2005) The three-dimensional solution structure of Ca(2+)-bound S100A1 as determined by NMR spectroscopy, *J Mol Biol* 353, 410-426.

3. Lee, Y.T., Dimitrova, Y.N., Schneider, G., Ridenour, W.B., Bhattacharya, S., Soss, S.E., Caprioli, R.M., Filipek, A., and Chazin, W.J. (2008) Structure of the S100A6 complex with a fragment from the C-terminal domain of Siah-1 interacting protein: a novel mode for S100 protein target recognition, *Biochemistry* 47, 10921-10932.

4. Zimmer, D.B., Chaplin, J., Baldwin, A., and Rast, M. (2005) S100-mediated signal transduction in the nervous system and neurological diseases, *Cell Mol Biol (Noisy-le-grand)* 51, 201-214.

5. Heizmann, C.W., Fritz, G., and Schafer, B.W. (2002) S100 proteins: structure, functions and pathology, *Front Biosci* 7, d1356-1368.

6. Rohde, D., Ritterhoff, J., Voelkers, M., Katus, H.A., Parker, T.G., and Most, P. (2010) S100A1: a multifaceted therapeutic target in cardiovascular disease, *J Cardiovasc Transl Res* 3, 525-537.

7. Kraus, C., Rohde, D., Weidenhammer, C., Qiu, G., Pleger, S.T., Voelkers, M., Boerries, M., Remppis, A., Katus, H.A., and Most, P. (2009) S100A1 in cardiovascular health and disease: closing the gap between basic science and clinical therapy, *J Mol Cell Cardiol* 47, 445-455.

8. Goch, G., Vdovenko, S., Kozlowska, H., and Bierzynski, A. (2005) Affinity of S100A1 protein for calcium increases dramatically upon glutathionylation, *FEBS J* 272, 2557-2565.

9. Ghezzi, P., Bonetto, V., and Fratelli, M. (2005) Thiol-disulfide balance: from the concept of oxidative stress to that of redox regulation, *Antioxid Redox Signal* 7, 964-972.

10. Dalle-Donne, I., Rossi, R., Colombo, G., Giustarini, D., and Milzani, A. (2009) Protein S-glutathionylation: a regulatory device from bacteria to humans, *Trends Biochem Sci* 34, 85-96.

11. Ghezzi, P. and Di Simplicio, P. (2009) *Protein glutationylation*, in *Redox signaling and regulation in biology and medicine* (C. Jacob and P.C. Winyard), pp 123-141, Wiley-VCH, Weinheim.

12. Palmer, A.G., 3rd (2004) NMR characterization of the dynamics of biomacromolecules, *Chem Rev* 104, 3623-3640.

13. Morin, S. (2011) A practical guide to protein dynamics from 15N spin relaxation in solution, *Prog Nucl Magn Reson Spectrosc* 59, 245-262.

14. Nowakowski, M., Jaremko, L., Jaremko, M., Zhukov, I., Belczyk, A., Bierzynski, A., and Ejchart, A. (2011) Solution NMR structure and dynamics of human apo-S100A1 protein, *J Struct Biol* 174, 391-399.

15. Finkelstein, J.D. (1998) The metabolism of homocysteine: pathways and regulation, *Eur J Pediatr* 157 Suppl 2, S40-44.

16. Hultberg, B., Andersson, A., and Isaksson, A. (1998) Protein binding of homocysteine and other thiols in HeLa cell cultures after addition of homocysteine and copper ions, *Clin Chim Acta* 269, 175-184.

17. Mansoor, M.A., Guttormsen, A.B., Fiskerstrand, T., Refsum, H., Ueland, P.M., and Svardal, A.M. (1993) Redox status and protein binding of plasma aminothiols during the transient hyperhomocysteinemia that follows homocysteine administration, *Clin Chem* 39, 980-985.

18. Nygard, O., Nordrehaug, J.E., Refsum, H., Ueland, P.M., Farstad, M., and Vollset, S.E. (1997) Plasma homocysteine levels and mortality in patients with coronary artery disease, *N Engl J Med* 337, 230-236.

19. Glushchenko, A.V. and Jacobsen, D.W. (2007) Molecular targeting of proteins by L-homocysteine: mechanistic implications for vascular disease, *Antioxid Redox Signal* 9, 1883-1898.

20. Kessler, H., Bleich, S., Falkai, P., and Supprian, T. (2003) [Homocysteine and dementia], *Fortschr Neurol Psychiatr* 71, 150-156.

21. Morris, M.S. (2003) Homocysteine and Alzheimer's disease, *Lancet Neurol* 2, 425-428.

22. Bolewska, K., Kozlowska, H., Goch, G., Mikołajek, B., and Bierzynski, A. (1997) Molecular cloning and expression in Escherichia coli of a gene coding for bovine S100A1 protein and its Glu32 Gln and Glu73 Gln mutants., *Acta Biochim. Polon.* 44, 275-284.

23. Dixon, M. and Webb, E.C. (1961) Enzyme fractionation by salting-out: a theoretical note, *Adv Protein Chem* 16, 197-219.

24. Falconer, J.S., Jenden, D.J., and Taylor, D.B. (1953) The application of solubility measurements to the study of complex protein solutions and to the isolation of individual proteins., *Discuss. Faraday Soc.* 13, 40-50.

25. Baldisseri, D.M., Rustandi, R.R., Zhang, Z., Tang, C., Bair, C.L., Landar, A., Zimmer, D.B., and Weber, D.J. (1999) 1H, 13C and 15N NMR sequence-specific resonance assignments for rat apo-S100A1(alpha alpha), *J Biomol NMR* 14, 91-92.

26. Marion, D., Ikura, M., Tschudin, R., and Bax, A. (1989) Rapid recording of 2D NMR spectra without phase cycling. Application to the study of hydrogen exchange in proteins., *J. Magn. Reson.* 85, 393-399.

27. Kay, L.E., Keifer, P., and Saarinen, T. (1992) Pure absorption gradient enhanced heteronuclear single quantum correlation spectroscopy with improved sensitivity, *J. Am. Chem. Soc.* 114, 10663-10665.

28. Wishart, D.S., Bigam, C.G., Yao, C.G., Abildgaad, F., Dyson, H.J., Oldfield, E., Markley, J.L., and Sykes, B.D. (1995) 1H, 13C and 15N chemical shift referencing in biomolecular NMR, *J. Biomol. NMR* 6, 135-140.

29. Delaglio, F., Grzesiek, S., Vuister, G.W., Zhu, G., Pfeifer, J., and Bax, A. (1995) NMRPipe: a multidimensional spectral processing system based on UNIX pipes, *J Biomol NMR* 6, 277-293.

30. www.cara.nmr.ch, Keller, R.L.J. *The computer aided resonance assignment tutorial*. 2004;

31. Goddard, T.D. and Kneller, D.G., *SPARKY3*: University of California, San Francisco.

32. Muhandiram, D.R. and Kay, L.E. (1994) Gradient-enhanced triple-resonance three-dimensional NMR experiments with improved sensitivity, *J. Magn. Reson. B* 103, 203-216.

33. Ikura, M., Kay, L.E., and Bax, A. (1990) A novel approach for sequential assignment of 1H, 13C, and 15N spectra of proteins: heteronuclear triple-resonance three-dimensional NMR spectroscopy. Application to calmodulin, *Biochemistry* 29, 4659-4667.

34. Bax, A. and Ikura, M. (1991) An efficient 3D NMR technique for correlating the proton and 15N backbone amide resonances with the alpha-carbon of the preceding residue in uniformly 15N/13C enriched proteins, *J Biomol NMR* 1, 99-104.

35. Wittekind, M. and Mueller, L. (1993) HNCACB, a high-sensivity 3D NMR experiment to correlate amide proton and nitrogen resonances with the alpha- and beta-carbon resonances in proteins, *J. Magn. Reson. B* 101, 201-205.

36. Grzesiek, S. and Bax, A. (1992) Correlating backbone amide and side chain resonances in larger proteins by multiple relayed triple resonance NMR, *J. Am. Chem. Soc.* 114, 6291-6293.

37. Lohr, F. and Ruterjans, H. (1995) A new triple-resonance experiment for the sequential assignment of backbone resonances in proteins, *J. Biomol. NMR* 6, 189-197.

38. Zhang, O., Kay, L.E., Olivier, J.P., and Forman-Kay, J.D. (1994) Backbone 1H and 15N resonance assignments of the N-terminal SH3 domain of drk in folded and unfolded

states using enhanced-sensitivity pulsed field gradient NMR techniques, *J. Biomol. NMR* 4, 845-858.

39. Grzesiek, S., Anglister, J., and Bax, A. (1993) Correlation of backbone amide and aliphatic side-chain resonances in 13C/15N-enriched proteins by isotropic mixing of 13C magnetization, *J Magn. Reson. B* 101, 114-119.

40. Grzesiek, S. and Bax, A. (1993) Amino acid type determination in the sequential assignment procedure of uniformly 13C/15N-enriched proteins, *J. Biomol. NMR* 3, 185-204.

41. Bax, A., Clore, G.M., and Gronenborn, A.M. (1990) 1H-1H correlation via isotropic mixing of 13C magnetization: a new three-dimensional approach for assigning 1H and 13C spectra of 13C-enriched proteins, *J. Magn. Reson.* 88, 425-431.

42. Muhandiram, D.R., Farrow, N.A., Xu, G.-Y., Smallcombe, S.H., and Kay, L.E. (1993) A gradient 13C NOESY-HSQC experiment for recording NOESY spectra of 13C-labeled proteins dissolved in H2O, J. Magn. Reson. B, 317-321.

43. Yamazaki, T., Forman-Kay, J.D., and Kay, L.E. (1993) Two-dimensional NMR experiments for correlating 13Cb and 1Hd/e chemical shifts of aromatic residues in 13C-labeled proteins via scalar couplings, *J. Am. Chem. Soc.* 115, 11054-11055.

44. Farrow, N.A., Muhandiram, R., Singer, A.U., Pascal, S.M., Kay, C.M., Gish, G., Shoelson, S.E., Pawson, T., Forman-Kay, J.D., and Kay, L.E. (1994) Backbone dynamics of a free and phosphopeptide-complexed Src homology 2 domain studied by 15N NMR relaxation, *Biochemistry* 33, 5984-6003.

45. Kay, L.E., Nicholson, L.K., Delaglio, F., Bax, A., and Torchia, D.A. (1992) Pulse schemes for removal of the effects of cross correlation between dipolar and chemical-shift

anisotropy relaxation mechanisms on the measurement of heteronuclear T1 and T2 values in proteins, *J. Magn. Reson.* 97, 359-375.

46. Fushman, D. (2003) *Determination of protein dynamics using 15N relaxation measurements*, in *BioNMR in Drug Research* (O. Zerbe), pp 283-308, Wiley-VCH, Weinheim.

47. Guntert, P., Mumenthaler, C., and Wuthrich, K. (1997) Torsion angle dynamics for NMR structure calculation with the new program DYANA, *J Mol Biol* 273, 283-298.

48. Herrmann, T., Guntert, P., and Wuthrich, K. (2002) Protein NMR structure determination with automated NOE-identification in the NOESY spectra using the new software ATNOS, *J Biomol NMR* 24, 171-189.

49. Guntert, P., Qian, Y.Q., Otting, G., Muller, M., Gehring, W., and Wuthrich, K. (1991) Structure determination of the Antp (C39----S) homeodomain from nuclear magnetic resonance data in solution using a novel strategy for the structure calculation with the programs DIANA, CALIBA, HABAS and GLOMSA, *J Mol Biol* 217, 531-540.

50. Berjanskii, M.V., Neal, S., and Wishart, D.S. (2006) PREDITOR: a web server for predicting protein torsion angle restraints, *Nucleic Acids Res* 34, W63-69.

51. Schwieters, C.D., Kuszewski, J.J., Tjandra, N., and Clore, G.M. (2003) The Xplor-NIH NMR molecular structure determination package, *J Magn Reson* 160, 65-73.

52. Laskowski, R.A., Rullmannn, J.A., MacArthur, M.W., Kaptein, R., and Thornton, J.M. (1996) AQUA and PROCHECK-NMR: programs for checking the quality of protein structures solved by NMR, *J Biomol NMR* 8, 477-486.

53. Vriend, G. (1990) WHAT IF: a molecular modeling and drug design program, *J Mol Graph* 8, 29, 52-26.

54. Clore, G.M., Szabo, A., Bax, A., Kay, L.E., Driscoll, P.C., and Gronenborn, A.M. (1990) Deviations from the simple two-parameter model-free approach to the interpretation of nitrogen-15 nuclear magnetic relaxation of proteins, *J. Am. Chem. Soc.* 112, 4989-4991.

55. Baber, J.L., Szabo, A., and Tjandra, N. (2001) Analysis of slow interdomain motion of macromolecules using NMR relaxation data, *J Am Chem Soc* 123, 3953-3959.

56. Tjandra, N., Kuboniwa, H., Ren, H., and Bax, A. (1995) Rotational dynamics of calcium-free calmodulin studied by 15N-NMR relaxation measurements, *Eur J Biochem* 230, 1014-1024.

57. Woessner, D.E. (1962) Nuclear spin relaxation in ellipsoid undergoing rotational Brownian motion, *J. Chem. Phys.* 37, 647-654.

58. Ottinger, M. and Bax, A. (1998) Determination of relative N-HN, N-C', Ca-C', and Ca-Ha effective bond lengths in a protein by NMR in a dilute liquid crystalline phase, *J. Am. Chem. Soc.* 120, 12334-12341.

59. Yao, L., Grishaev, A., Cornilescu, G., and Bax, A. (2010) Site-specific backbone amide (15)N chemical shift anisotropy tensors in a small protein from liquid crystal and cross-correlated relaxation measurements, *J Am Chem Soc* 132, 4295-4309.

60. Alexandrescu, A.T. and Shortle, D. (1994) Backbone dynamics of a highly disordered 131 residue fragment of staphylococcal nuclease, *J Mol Biol* 242, 527-546.

61. Brutscher, B., Bruschweiler, R., and Ernst, R.R. (1997) Backbone dynamics and structural characterization of the partially folded A state of ubiquitin by 1H, 13C, and 15N nuclear magnetic resonance spectroscopy, *Biochemistry* 36, 13043-13053.

62. Press, W.H., Flannery, B.P., Teukolsky, S.A., and Vetterling, W.T. (1986) in *Numerical recipes. The art of scientific computing*, Cambridge University Press, Cambridge.

63. Martin, O.A., Villegas, M.E., Vila, J.A., and Scheraga, H.A. (2010) Analysis of 13Calpha and 13Cbeta chemical shifts of cysteine and cystine residues in proteins: a quantum chemical approach, *J Biomol NMR* 46, 217-225.

64. Sharma, D. and Rajarathnam, K. (2000) 13C NMR chemical shifts can predict disulfide bond formation, *J Biomol NMR* 18, 165-171.

65. Bertini, I., Das Gupta, S., Hu, X., Karavelas, T., Luchinat, C., Parigi, G., and Yuan, J. (2009) Solution structure and dynamics of S100A5 in the apo and Ca2+-bound states, *J Biol Inorg Chem* 14, 1097-1107.

66. Dutta, K., Cox, C.J., Basavappa, R., and Pascal, S.M. (2008) 15N relaxation studies of Apo-Mts1: a dynamic S100 protein, *Biochemistry* 47, 7637-7647.

67. Inmam, K.G., Baldisseri, D.M., Miller, K.E., and Weber, D.J. (2001) Backbone dynamics of the calcium-signaling protein apo-S100B as determined by 15N NMR relaxation, *Biochemistry* 40, 3439-3448.

68. Zhukov, I., Ejchart, A., and Bierzynski, A. (2008) Structural and motional changes induced in apo-S100A1 protein by the disulfide formation between its Cys 85 residue and beta-mercaptoethanol, *Biochemistry* 47, 640-650.

69. Rustandi, R.R., Baldisseri, D.M., Inman, K.G., Nizner, P., Hamilton, S.M., Landar, A., Zimmer, D.B., and Weber, D.J. (2002) Three-dimensional solution structure of the calcium-signaling protein apo-S100A1 as determined by NMR, *Biochemistry* 41, 788-796.

70. Otterbein, L.R., Kordowska, J., Witte-Hoffmann, C., Wang, C.L., and Dominguez, R. (2002) Crystal structures of S100A6 in the Ca(2+)-free and Ca(2+)-bound states: the calcium sensor mechanism of S100 proteins revealed at atomic resolution, *Structure* 10, 557-567.

71. Wright, N.T., Prosser, B.L., Varney, K.M., Zimmer, D.B., Schneider, M.F., and Weber, D.J. (2008) S100A1 and calmodulin compete for the same binding site on ryanodine receptor, *J Biol Chem* 283, 26676-26683.

72. Wright, N.T., Cannon, B.R., Wilder, P.T., Morgan, M.T., Varney, K.M., Zimmer, D.B., and Weber, D.J. (2009) Solution structure of S100A1 bound to the CapZ peptide (TRTK12), *J Mol Biol* 386, 1265-1277.

73. Smith, S.P. and Shaw, G.S. (1997) Assignment and secondary structure of calcium-bound human S100B, *J Biomol NMR* 10, 77-88.

74. Drohat, A.C., Baldisseri, D.M., Rustandi, R.R., and Weber, D.J. (1998) Solution structure of calcium-bound rat S100B(betabeta) as determined by nuclear magnetic resonance spectroscopy, *Biochemistry* 37, 2729-2740.

75. Koch, M. and Fritz, G. (2012) The structure of Ca2+-loaded S100A2 at 1.3-A resolution, *FEBS J* 279, 1799-1810.

76. Rety, S., Osterloh, D., Arie, J.P., Tabaries, S., Seeman, J., Russo-Marie, F., Gerke, V., and Lewit-Bentley, A. (2000) Structural basis of the Ca(2+)-dependent association between S100C (S100A11) and its target, the N-terminal part of annexin I, *Structure* 8, 175-184.

77. Gingras, A.R., Basran, J., Prescott, A., Kriajevska, M., Bagshaw, C.R., and Barsukov, I.L. (2008) Crystal structure of the Ca(2+)-form and Ca(2+)-binding kinetics of metastasis-associated protein, S100A4, *FEBS Lett* 582, 1651-1656.

78. Drohat, A.C., Amburgey, J.C., Abildgaard, F., Starich, M.R., Baldisseri, D., and Weber, D.J. (1996) Solution structure of rat apo-S100B(beta beta) as determined by NMR spectroscopy, *Biochemistry* 35, 11577-11588.

Table 1. NMR-derived constraints and statistics for human *holo*-S100A1 and *holo*-S100A1-Hcy proteins calculated with XPLOR-NIH 2.26

NOE distance constraints within subunit	1193	1240
Intraresidual & sequential ($\|i-j\|\leq 1$)	713	723
Medium-range ($1<\|i-j\|<5$)	302	270
Long-range ($\|i-j\|\geq 5$)	178	247
Intersubunit NOE distance constraints per subunit	121	158
Hydrogen bond constraints	29	50
Restraints per residue	14.4	15.6
Restraints for Ca^{2+} ion per subunit	10	10
Torsion angle constraints:		
Backbone (φ/ψ)	74/71	67/67
Side chains (χ^1/χ^2)	0/0	0/0
Mean r.m.s.d. from experimental restraints (±s.d.)		
NOE (Å)	0.0126 ± 0.0012	0.0192 ± 0.0013
Dihedral angles (deg)	1.13 ± 0.20	0.59 ± 0.08
r.m.s.d. from idealized covalent geometry (region 1..93)(±s.d.)		
Bonds (Å)	0.0038 ± 0.0003	0.0056 ± 0.0003
Angles (deg)	0.68 ± 0.03	0.84 ± 0.02
Impropers (deg)	0.56 ± 0.03	0.65 ± 0.02
Ramachandran plot (1..93)		
Residues in the most favored regions (%)	95.1	95.9
Residues in additional allowed regions (%)	4.1	3.7
Residues in generously allowed regions (%)	0.6	0.2
Residues in disallowed regions (%)	0.2	0.2
Ramachandran plot (5..85)		
Residues in the most favored regions (%)	94.4	95.7
Residues in additional allowed regions (%)	4.6	4.0

Residues in generously allowed regions (%)	0.7	0.1
Residues in disallowed regions (%)	0.3	0.2
r.m.s.d. to the mean subunit structure		
Ordered backbone atoms (1..93) (Å)	1.06 ± 0.25	0.84 ± 0.20
Ordered heavy atoms (1..93) (Å)	1.70 ± 0.26	1.19 ± 0.17
Ordered backbone atoms (5..85) (Å)	0.86 ± 0.22	0.44 ± 0.10
Ordered heavy atoms (5..85) (Å)	1.49 ± 0.26	0.85 ± 0.12
r.m.s.d. to the mean structure of the whole dimer (both subunits)		
Ordered backbone atoms (1..93) (Å)	1.17 ± 0.29	0.89 ± 0.20
Ordered heavy atoms (1..93) (Å)	1.78 ± 0.29	1.13 ± 0.17
Ordered backbone atoms (5..85) (Å)	0.94 ± 0.22	0.54 ± 0.14
Ordered heavy atoms (5..85) (Å)	1.54 ± 0.27	1.04 ± 0.15
Structure Z-scores		
1st generation packing quality	2.081 ± 0.525	2.088 ± 0.451
2nd generation packing quality	4.573 ± 1.451	3.885 ± 1.278
Ramachandran plot appearance	1.687 ± 0.364	1.954 ± 0.319
χ^1 and χ^2 rotamer normality	2.010 ± 0.438	0.369 ± 0.412
Backbone conformation	0.647 ± 0.504	-0.181 ± 0.200
Equivalent X-ray resolution of Ramachandran plot (1..93) (Å)	1.0	1.0
Equivalent X-ray resolution of Ramachandran plot (5..85) (Å)	1.0	1.0
Equivalent X-ray resolution of χ^1 and χ^2 (1..93) (Å)	1.0/1.0	1.1/1.0

Table 2. Angles (in degrees) between helices I, II, III and IV in human and rat S100A1 structures[a].

Helices	human *apo*-S100A1[b]	rat *holo*-S100A1[c]	human *holo*-S100A1[d]	human *holo*-S100A1-Hcy[e]
I → II	133 ± 1	132 ± 1	132 ± 2	139 ± 1
I → IV	117 ± 1	131 ± 2	119 ± 2	130 ± 1
II → IV	–34 ± 1	–29 ± 1	–26 ± 3	-35 ± 1
I → I'	–144 ± 2	–157 ± 3	–158 ± 2	–154 ± 1
IV → IV'	151 ± 1	152 ± 3	144 ± 6	149 ± 1
III → IV	-167 ± 2	121 ± 2	130 ± 4	112 ± 2

[a] Interhelical angles were calculated using interhlx (K. Yap, University of Toronto).

[b] Taken from NMR structure (PDB entry 2L0P).

[c] Taken from NMR structure (PDB entry 1ZFS).

[d] Taken from NMR structure (PDB entry 2LP3), this work.

[e] Taken from NMR structure (PDB entry 2LP2), this work.

Sign of the interhelical angle was chosen according to convention proposed in [78].

Figure captions

Figure 1. $^{1}H–^{15}N$ HSQC spectrum of human *holo*-S100A1 protein. The terminal NH_2 groups of Asn and Gln residues are not labeled. One of two cross peaks labeled W90 at 9.621/128.53 corresponds to side chain NH group of indol moiety.

Figure 2. Ribbon representations of the *holo*-S100A1 (A) and *holo*-S100A1-Hcy - (B) structures. Subsequent helices of EF-hand motifs are colored: helix I - blue, helix II - cyan, helix III - red and helix IV - yellow. Calcium ions are shown as spheres and homocysteine in stick representation.

Figure 3. Weighted means of generalized order parameter values $<S^2>$ with corresponding error bars for amino acid residues in various structural elements of human *holo*-S100A1 and *holo*-S100A1-Hcy proteins compared with corresponding values obtained for *apo*-S100A1 [14]. Relaxation data were analyzed assuming fully anisotropic overall tumbling [57] and extended model-free spectral density functions [54].

Figure 4. Data (vertical bars) for exchange terms R_{ex} at 9.4 T with corresponding error bars for human *apo*-S100A1 (A) *holo*-S100A1 (B) and *holo*-S100A1-Hcy (C) proteins vs. residue number. Insignificant R_{ex} values smaller than 0.5 s^{-1} and, therefore, close to their accuracy are shown as hatched bars. The horizontal lines indicate positions of four helices in EF-hand motifs.

Figure 5. Comparison of most representative structures for human *holo*-S100A1 (red) and *apo*-S100A1 (blue) proteins. Calcium ions are represented as yellow spheres.

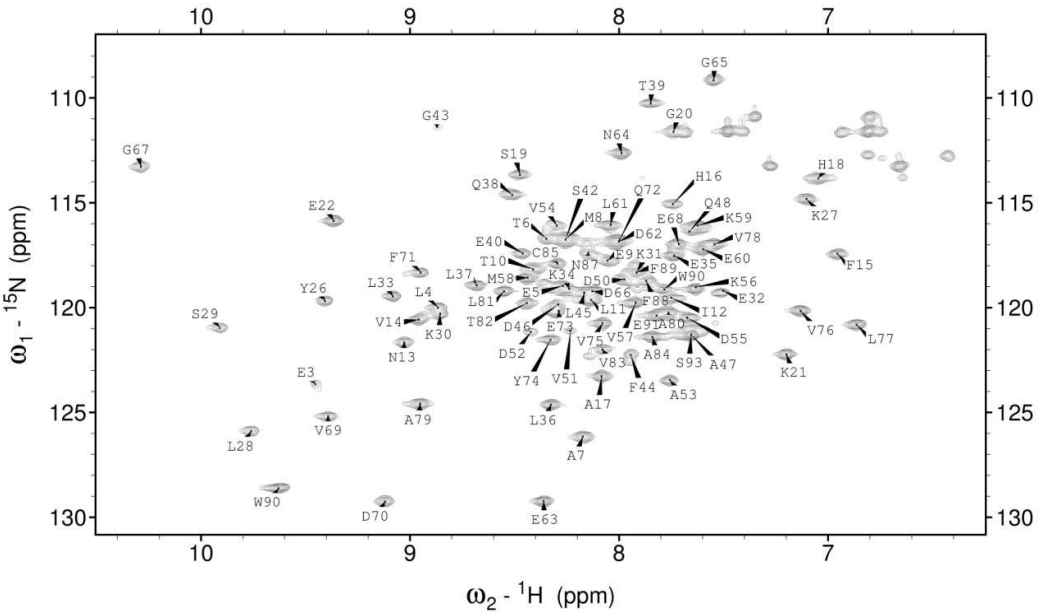
10
9
8
7
110
115
120
125
130
ω_1 - ^{15}N (ppm)
ω_2 - ^{1}H (ppm)
G65
T39
G20
G43
N64
G67
S19
H16
H18
Q38
S42
Q72
Q48
K59
K27
E22
V54
L61
M8
E68
T6
D62
V78
E40
C85
E9
K31
E60
F15
F71
T10
N87
E35
L37
M58
K34
F89
W90
K56
D50
Y26
L33
L4
E5
D66
E32
L81
F88
I12
S29
L45
L11
V14
T82
D46
E73
E91
A80
V76
L77
K30
D55
V75
V57
N13
D52
A84
S93
A47
K21
E3
Y74
V51
V83
F44
A53
A17
A79
L36
V69
L28
A7
W90
D70
E63

Figure 1

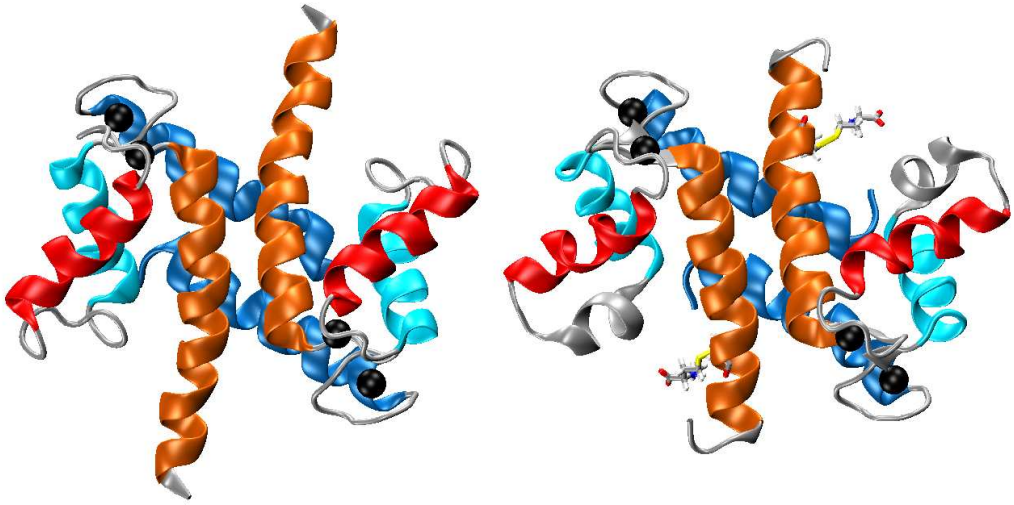

Figure 2

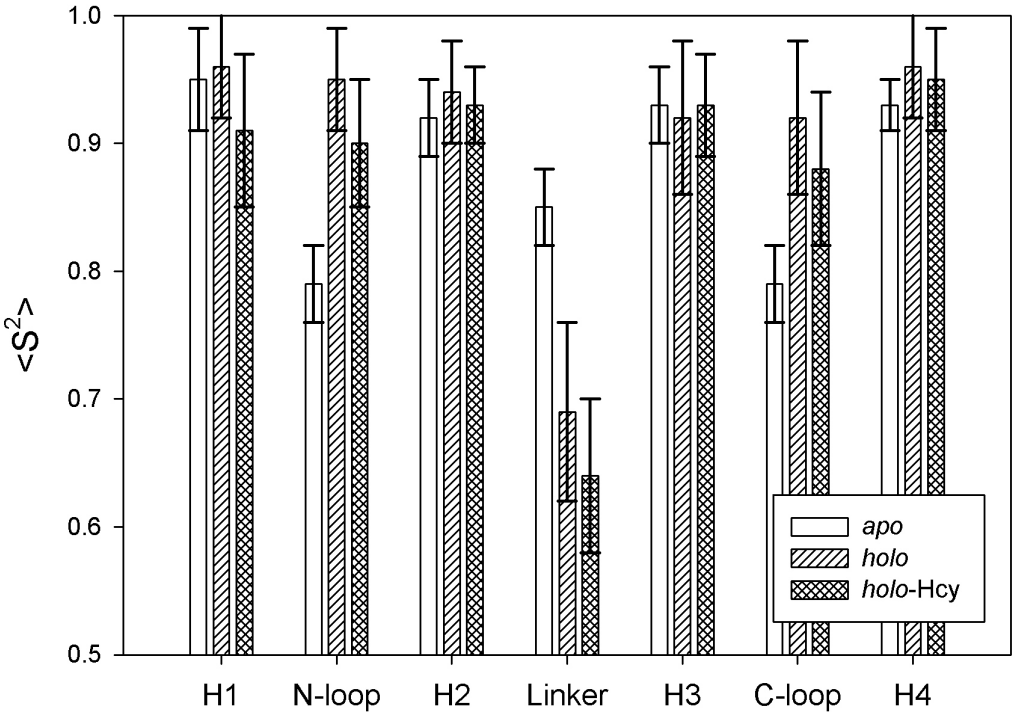
1.0
0.9
0.8
0.7
0.6
0.5
<S2>
H1
N-loop
H2
Linker
H3
C-loop
H4
apo
holo
holo-Hcy

Figure 3

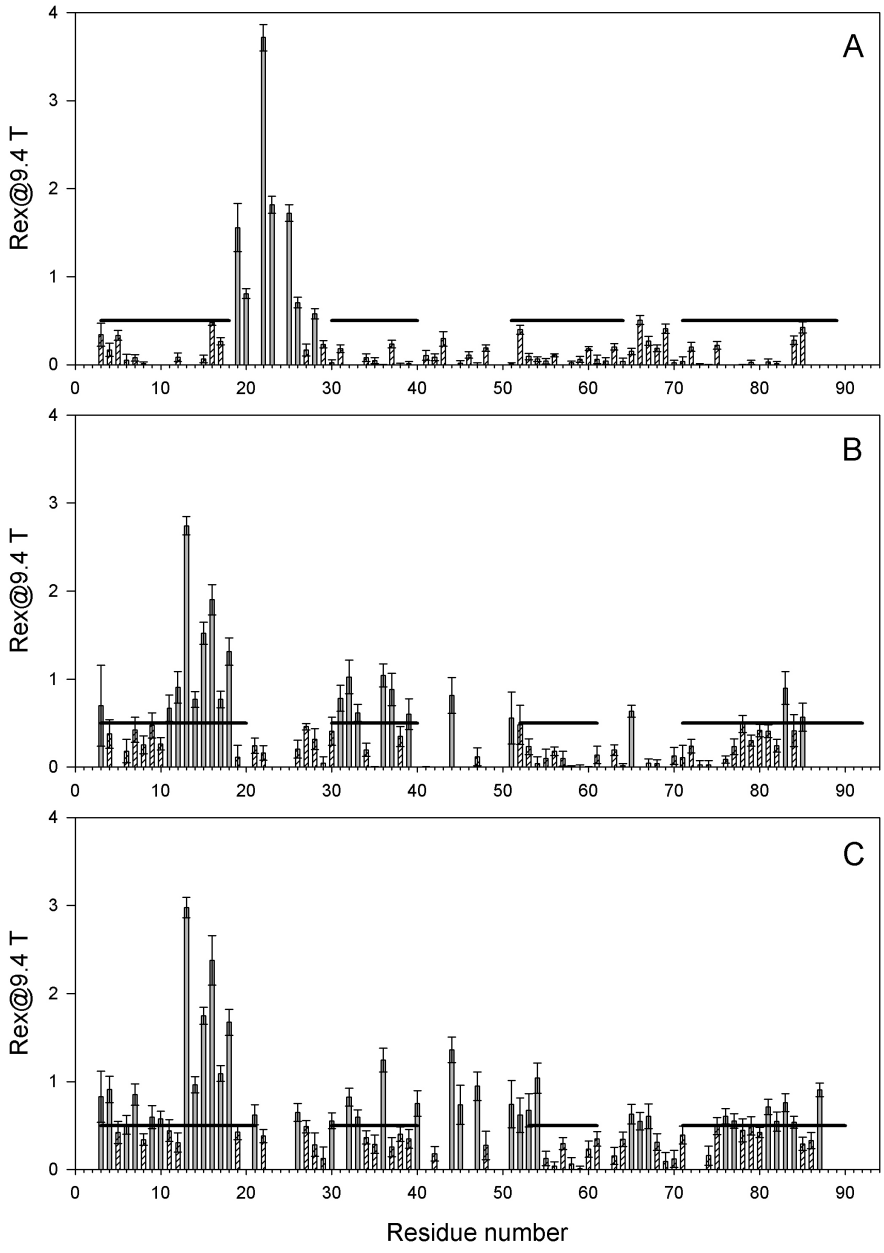

Figure 4

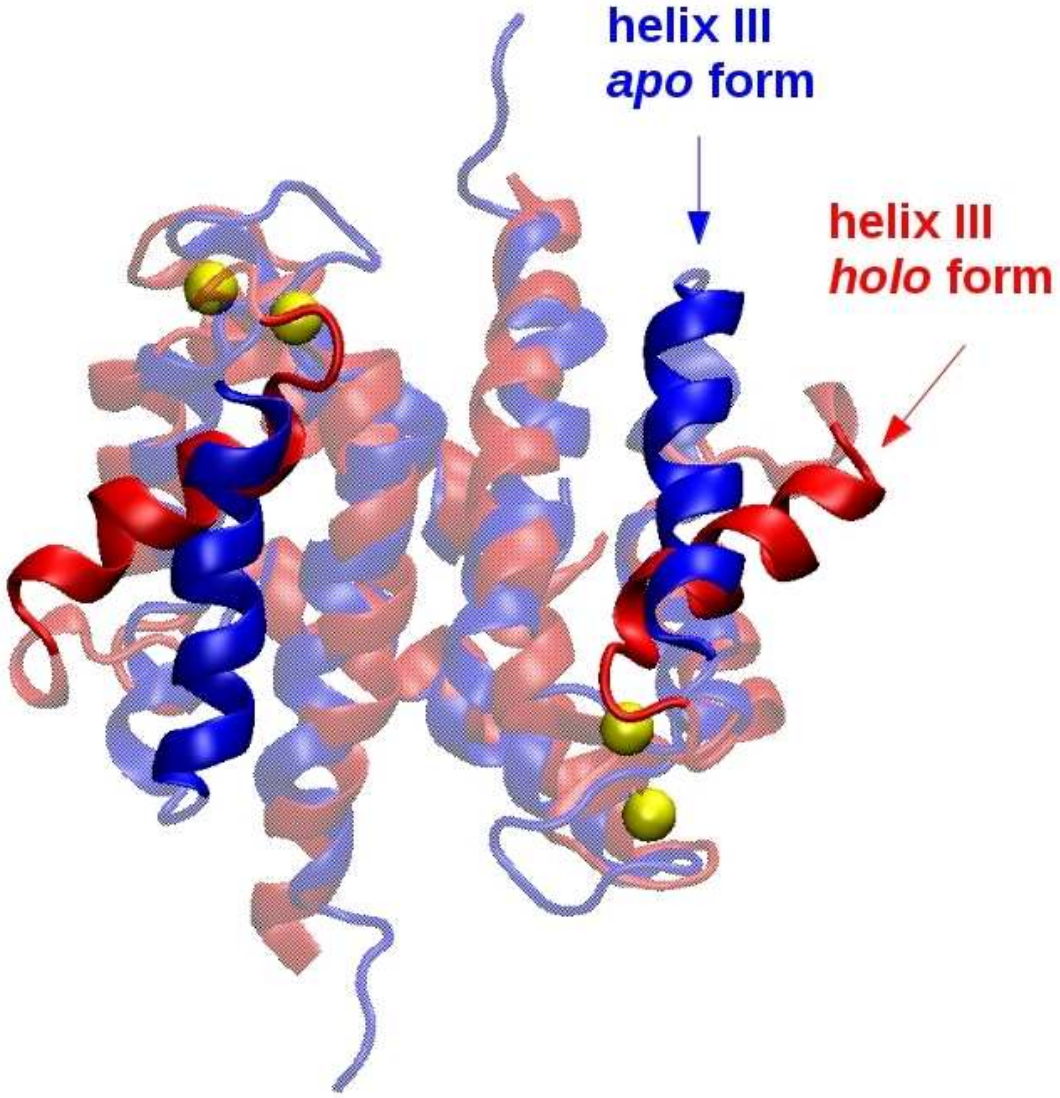

Figure 5

Table of contents use only

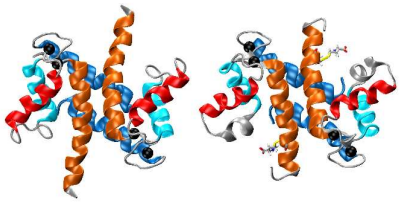

Impact of calcium binding and thionylation of S100A1 protein on its NMR derived structure and backbone dynamics

Michał Nowakowski, Katarzyna Ruszczyńska-Bartnik, Monika Budzińska, Łukasz Jaremko, Mariusz Jaremko, Konrad Zdanowski, Andrzej Bierzyński, and Andrzej Ejchart